01 Dec 2019

Lattice Thermal Conductivity of Quartz at High Pressure and Temperature from the Boltzmann Transport Equation

Xue Xiong

Eugene J. Ragasa

Aleksandr V. Chernatynskiy
Missouri University of Science and Technology, aleksandrc@mst.edu

Dawei Tang

et. al. For a complete list of authors, see https://scholarsmine.mst.edu/phys_facwork/2041

Recommended Citation

X. Xiong et al., "Lattice Thermal Conductivity of Quartz at High Pressure and Temperature from the Boltzmann Transport Equation," *Journal of Applied Physics*, vol. 126, no. 21, American Institute of Physics (AIP), Dec 2019.
The definitive version is available at https://doi.org/10.1063/1.5114992

Journal of Applied Physics ARTICLE scitation.org/journal/jap

Lattice thermal conductivity of quartz at high pressure and temperature from the Boltzmann transport equation

Cite as: J. Appl. Phys. **126**, 215106 (2019); doi: 10.1063/1.5114992
Submitted: 13 June 2019 · Accepted: 14 November 2019 ·
Published Online: 2 December 2019

Xue Xiong (熊雪),[1,2,3] Eugene J. Ragasa,[3] Aleksandr Chernatynskiy,[4] Dawei Tang (唐大伟),[5,a)] and Simon R. Phillpot[3,a)]

AFFILIATIONS

[1]Institute of Engineering Thermophysics, Chinese Academy of Sciences, Beijing 100190, China
[2]University of Chinese Academy of Sciences, Beijing 100049, China
[3]Department of Materials Science and Engineering, University of Florida, Gainesville, Florida 32611, USA
[4]Department of Physics, Missouri University of Science and Technology, Rolla, Missouri 65409, USA
[5]Key Laboratory of Ocean Energy Utilization and Energy Conservation of Ministry of Education, Dalian University of Technology, Dalian 116024, China

[a)]**Authors to whom correspondence should be addressed:** dwtang@dlut.edu.cn and sphil@mse.ufl.edu

ABSTRACT

The thermal conductivities along the basal and hexagonal directions of α-quartz silica, the low-temperature form of crystalline SiO_2, are predicted from the solution of the Boltzmann transport equation combined with the van Beest, Kramer, and van Santen potential for the temperature up to 900 K and the pressure as high as 4 GPa. The thermal conductivities at atmospheric pressure, which show a negative and nonlinear dependence on temperature, are in reasonable agreement with the experimental data. The influence of pressure on thermal conductivity is positive and linear. The pressure (P) and temperature (T) dependences of the thermal conductivity (λ) in basal and hexagonal directions are fitted to a function of the form $\lambda = (b + cP)T^a$. The thermal conductivity, influenced by temperature and pressure, is analyzed based on phonon properties, including spectral thermal conductivity, dispersion relation, phonon density of states, phonon lifetime, and phonon probability density distribution function.

I. INTRODUCTION

Knowledge of thermal conductivity of Earth's crust and its dependence on temperature and pressure is required for quantitative calculations in geology and geophysics problems.[1,2] Since the properties of Earth rocks can be estimated based on those of the constituent minerals, the thermal conductivities of rock-forming minerals need to be systematically understood.[2]

Silicon dioxide is an appropriate prototype for the study of thermal conductivity, as silicon dioxide and silicate network materials are the largest component in the Earth's crust, with more than 60 mass %.[3–5] Quartz is the low-temperature polymorph of silica. Thus, there have been several simulations and experiments focused on the thermal conductivity of quartz and its temperature dependence on atmospheric pressure.[6–9] Nonequilibrium molecular dynamics (NEMD) has been used to calculate the thermal conductivity of quartz along the optical ([0001]) axis over a wide temperature range, with the interatomic interactions described by either the van Beest, Kramer, and van Santen (BKS) potential[7] or the third-generation Charge Optimized Many-Body (COMB3) potential.[10] Equilibrium molecular dynamics based on the Green-Kubo method has also been applied to predict the thermal conductivity of α-quartz from 100 K to 350 K.[8] All the results above were in good agreement with the experimental values.[6,9] Most of the experimental measurements of thermal conductivity of quartz were performed decades ago. Steady-state methods were most commonly used to determine the values in the directions perpendicular and parallel to the optical axis,[11–13] with the widest temperature range being from 300 K to 1000 K.[9]

The only work characterizing the effect of pressure on the thermal conductivity of silica was an experiment using the steady-state parallel-plate method on an amorphous sample in the temperature range from 273 K to 1273 K and at pressures up to 400 MPa.[14] However, the maximum pressure, 400 MPa, is much lower than the maximum pressure in the crust. The numerous theoretical methods available to calculate the thermal conductivity can provide an alternative to the experimental techniques. The published high-pressure simulations have focused on another important constituent mineral of rocks, MgO periclase, at high temperature and pressure.[15–17] However, there have not been any simulation studies of the thermal conductivity of quartz at high pressure.

In this paper, we determine the thermal conductivity of α-quartz silica as a function of temperature and pressure by solving the Boltzmann transport equation (BTE), with the interatomic interactions described by the BKS potential. The temperature range from 300 K to 900 K and the pressure range from 0 GPa to 4 GPa are chosen because the temperature and pressure of the crust increase with depth, reaching the maximum value of 500 °C (773 K) and 5 GPa at the crust-mantle boundary.[18]

II. METHODOLOGY

A. Structure

The structure of α-quartz silica is shown in Figs. 1(a)–1(d) from various perspectives, with the silicon atoms marked in blue and oxygen atoms in red. The experimental value of the Si–O–Si bond angle is 143.61°.[19] The structure consists of a continuous framework of corner-sharing SiO_4 tetrahedra connected through oxygen, as depicted in Fig. 1(d). The crystal symmetry of the unit cell is trigonal, belonging to the $P3_121$ space group. There are 3 silicon atoms and 6 oxygen atoms in the unit cell. The structure of high-temperature β-quartz is similar, except that the Si–O–Si bond angle is larger, with the experimental value being around 150°.[19] This also has the effect of increasing the overall symmetry: β-quartz has the same number of atoms in the unit cell and belongs to the hexagonal system with space group $P6_222$.

For computational convenience, we use an orthorhombic cell of 18 atoms as shown in Fig. 1(a) rather than the primitive trigonal unit cell of 9 atoms in our calculations and simulations. The orthorhombic simulation cell is described by the three length parameters a, b, and c. The basal a lattice parameters are the same in the hexagonal and orthorhombic cells, as are the values of c. The lattice parameter b in the orthorhombic cell is $\sqrt{3}$ times larger than in the hexagonal unit cell.

B. Temperature and pressure dependence of lattice parameters

The lattice parameters of the orthorhombic cell at various temperatures and pressures were computed by molecular dynamics (MD) and the classical BKS interatomic potential, which are used throughout this work. The details of the BKS potential can be found in the original BKS reference.[20] The influence of potential cutoff was tested by comparing the thermal conductivity calculated using 10 Å and 15 Å cutoffs: the difference was less than 1%, so the original value in reference 10 Å was used in all calculations. A supercell consisting of 2250 atoms was equilibrated at the specified temperature and pressure for 200 ps. The results were averaged over the last 5 ps; 10 independent calculations with different initial atomic velocity distributions were performed for each temperature and pressure. The lattice parameters determined by MD are expected to be more accurate than those determined

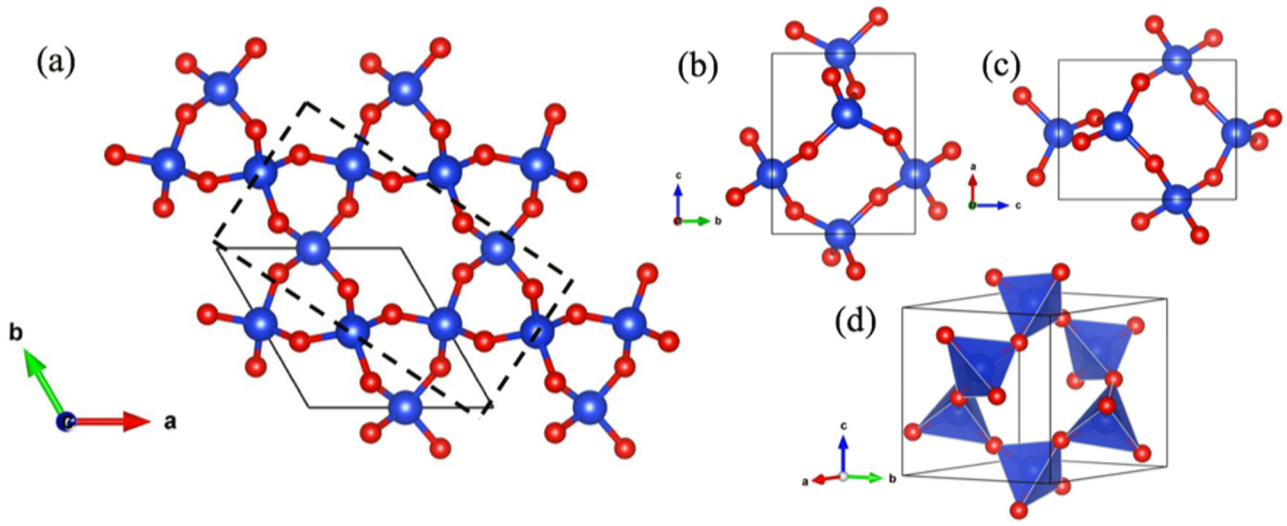

FIG. 1. The structure of the trigonal unit cell of α-quartz silica, oxygen atoms in red, silicon atoms in blue, from various perspectives. (a) along the direction parallel to [0001]. The box of the hexagonal unit cell is shown as a solid line, while the orthorhombic unit cell is outlined by the dashed line. (b) along the direction parallel to [1000], (c) along the direction parallel to [0100], and (d) perspective view showing the corner-sharing oxygen tetrahedra.

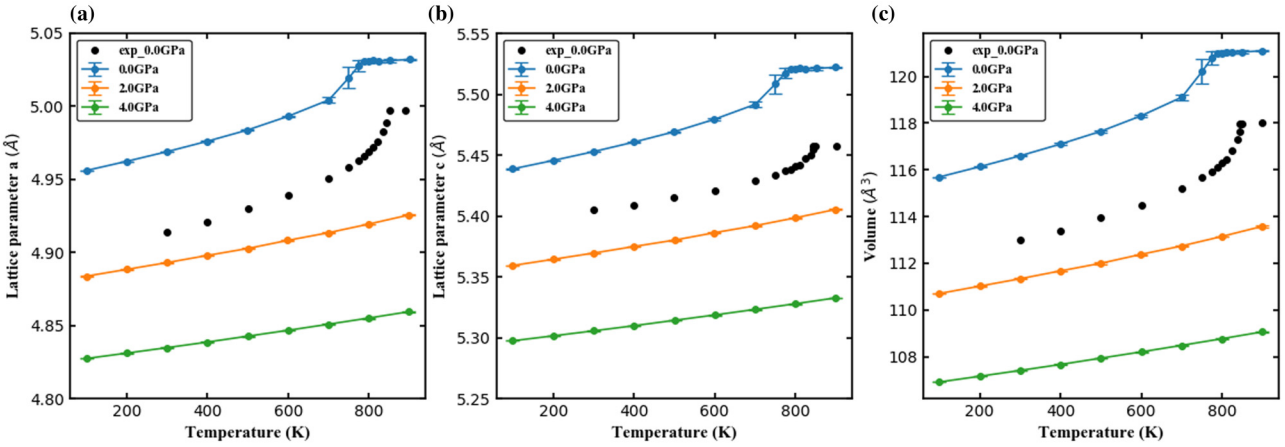

FIG. 2. Temperature dependence of lattice constants (*a* and *c*) and volume of molecular dynamics simulation in comparison with the experimental results[21] (black), for pressures of 0 GPa (blue), 2 GPa (orange), and 4 GPa (green).

from lattice dynamics, which offers only an incomplete description of the anharmonic effects of temperature.

The calculated lattice constants (*a* and *c*) and volume are shown in Fig. 2 as a function of temperature and pressure and compared with the experimental results.[21] Except for the precise value of the transition temperature, the simulations have a similar trend as the experiment. However, the cell volume is about 3% larger than the experiments. The thermal expansion and volume compression caused by pressure are clearly demonstrated. The discrete jump in lattice parameters between 700 K and 800 K for 0 GPa corresponds to the phase transition from α-quartz to β-quartz, as verified by an analysis of the radial and angular distribution functions. In particular, the radial distribution functions show that both second- and third-nearest peaks split, with the resulting subpeaks emerging above the transition.[22] The phase transition temperature determined from this simulation is 788 ± 12 K at zero pressure. This compares well with other studies using the BKS potential, which estimate the transition temperature to be 740 K[23] or 900 K.[22] The value from our simulation is less than 10% lower than the experimental value of 845 K (at an atmospheric pressure of 0.1 MPa).[22] Coesite is a high-pressure polymorph of silica and has been found in metamorphic rocks.[24] However, no transition from α-quartz to coesite has been observed.[25]

C. Thermal conductivity

The thermal conductivity is calculated from the solution of the Boltzmann transport equation (BTE) using the PhonTS Package.[26] Details of the theory and solution method are described in Ref. 27. Here, we briefly summarize those aspects salient to this analysis.

The thermal conductivity can be calculated based on Fourier's law and the expression for the heat current in terms of the distribution function $f_{\vec{k},n}$,

$$\vec{q} = \lambda \nabla T = \sum_{\vec{k},n} \hbar \omega_{\vec{k},n} \vec{v}_{\vec{k},n} f_{\vec{k},n}. \tag{1}$$

In this equation, ∇T is the temperature gradient; the phonon branch index n and the phonon wave vector $\vec{k}$ label the phonon state. $\omega_{\vec{k},n}$ is the phonon frequency, $\vec{v}_{\vec{k},n}$ is the phonon group velocity, and $f_{\vec{k},n}$ is the phonon distribution function. The phonon frequencies $\vec{\omega}_{\vec{k},n}$ are obtained in the usual manner by diagonalizing the dynamical matrix. The phonon group velocities are the gradients of the phonon frequencies as a function of the wave vector $\vec{k}$. The probability distribution functions $f_{\vec{k},n}$ can be calculated from the Boltzmann transport equation.

The canonical form of the linearized BTE for phonons is

$$-\vec{v}_{\vec{k},n} \cdot \frac{\partial f^0_{\vec{k},n}}{\partial T} \nabla T = \frac{1}{k_B T} \sum_{\vec{k}',n';\vec{k}'',n''} \left[\left(\Phi_{\vec{k},n} + \Phi_{\vec{k}',n'} - \Phi_{\vec{k}'',n''} \right) \Lambda^{\vec{k}'',n''}_{\vec{k},n;\vec{k}',n'} + \frac{1}{2} \left(\Phi_{\vec{k},n} - \Phi_{\vec{k}',n'} - \Phi_{\vec{k}'',n''} \right) \Lambda^{\vec{k}',n';\vec{k}'',n''}_{\vec{k},n;} \right], \tag{2}$$

where Λ is the equilibrium transition rate for three-phonon process and $\Phi_{\vec{k},n}$ is a small deviation of the probability distribution function $f_{\vec{k},n}$ from the equilibrium distribution function $f^0_{\vec{k},n}$ defined as

$$f_{\vec{k},n} = f^0_{\vec{k},n} - \frac{\partial f^0_{\vec{k},n}}{\partial(\hbar\omega)} \Phi_{\vec{k},n}. \tag{3}$$

In Eq. (2), the left-hand side represents phonon diffusion induced by the thermal gradient, while the right-hand side represents the scattering term for the three-phonon processes. Higher order interactions (i.e., processes involving four or more phonons) are not considered, though the importance of their effects is assessed below. The transition rates Λ are proportional to the square of the Fourier transform of the third derivative of the total potential energy with respect to the atom positions (third-order force constants). The detailed formulas and computation method of the transition rates can be found in Refs. 19 and 20.

We use the iterative method to solve the Boltzmann equation [Eq. (2)], representing the deviation of the distribution function $\Phi_{\vec{k},n}$ as

$$\Phi_{\vec{k},n} = \vec{F}_{\vec{k},n} \cdot \nabla T. \tag{4}$$

Substituting into Eq. (2) yields

$$\vec{F}_{\vec{k},n} = -\frac{\hbar\omega_{\vec{k},n} f^0_{\vec{k},n}\left(1+f^0_{\vec{k},n}\right)\vec{v}_{\vec{k},n}}{TQ_{\vec{k},n}} + \frac{1}{Q_{\vec{k},n}} \sum_{\vec{k}',n';\vec{k}'',n''} \left[\left(\vec{F}_{\vec{k}',n''} - \vec{F}_{\vec{k}',n'}\right)\Lambda^{\vec{k}'',n''}_{\vec{k},n;\vec{k}',n'} + \frac{1}{2}\left(\vec{F}_{\vec{k}',n'} + \vec{F}_{\vec{k}'',n''}\right)\Lambda^{\vec{k}',n';\vec{k}'',n''}_{\vec{k},n;}\right], \tag{5}$$

$$Q_{\vec{k},n} = \sum_{\vec{k}',n';\vec{k}'',n''} \left[\Lambda^{\vec{k}'',n''}_{\vec{k},n;\vec{k}',n'} + \frac{1}{2}\Lambda^{\vec{k}',n';\vec{k}'',n''}_{\vec{k},n;}\right]. \tag{6}$$

The numerical iteration method is used to solve to self-consistency,

$$\vec{F}^{i+1}_{\vec{k},n} = \vec{F}^0_{\vec{k},n} + \frac{1}{Q_{\vec{k},n}} \sum_{\vec{k}',n';\vec{k}'',n''} \left[\left(\vec{F}^i_{\vec{k}'',n''} - \vec{F}^i_{\vec{k}',n'}\right)\Lambda^{\vec{k}'',n''}_{\vec{k},n;\vec{k}',n'} + \frac{1}{2}\left(\vec{F}^i_{\vec{k}',n'} + \vec{F}^i_{\vec{k}'',n''}\right)\Lambda^{\vec{k}',n';\vec{k}'',n''}_{\vec{k},n;}\right]. \tag{7}$$

With the initial condition

$$\vec{F}^0_{\vec{k},n} = -\frac{\hbar\omega_{\vec{k},n} f^0_{\vec{k},n}\left(1+f^0_{\vec{k},n}\right)\vec{v}_{\vec{k},n}}{TQ_{\vec{k},n}}, \qquad \vec{F}^1_{\vec{k},n} = 0. \tag{8}$$

Once $|\vec{F}^{i+1}_{\vec{k},n} - \vec{F}^i_{\vec{k},n}|$ is below a specified value, the distribution is considered to be converged. Substituting the definition of $\vec{F}_{\vec{k},n}$ into Eq. (1), the final formalism of thermal conductivity is

$$\lambda = -\int \sum_n \hbar\omega_{\vec{k},n} \frac{f^0_{\vec{k},n}\left(1+f^0_{\vec{k},n}\right)}{k_B T} \vec{v}_{\vec{k},n} \otimes \vec{F}_{\vec{k},n} d\vec{k}. \tag{9}$$

Because of numerical limitations, the off diagonal components of λ are generally nonzero but are much smaller than the diagonal components.

For the orthorhombic simulation cell, the length b is the largest and the difference between the other two (a and c) is relatively small; for example, at 300 K and 0 GPa, $a = 4.969$ Å, $b = 8.607$ Å, and $c = 5.446$ Å. Therefore, a $11 \times 7 \times 11$ k-grid is used in the phonon Brillouin zone, with an additional 10 times denser grid along the c direction used to obtain better approximations to the energy and momentum conservation, resulting in improved convergence.[26] For the second and third derivatives of the total potential energy with respect to atom positions, the analytical differentiation of the BKS potential was used due to the relatively simple expression of the Buckingham type potential. The convergence of thermal conductivity as a function of iteration step is shown in Fig. 3. We found that the differences between the results of one and ten iterations were less than 2.5%; hence just one step for the iteration procedure was used.

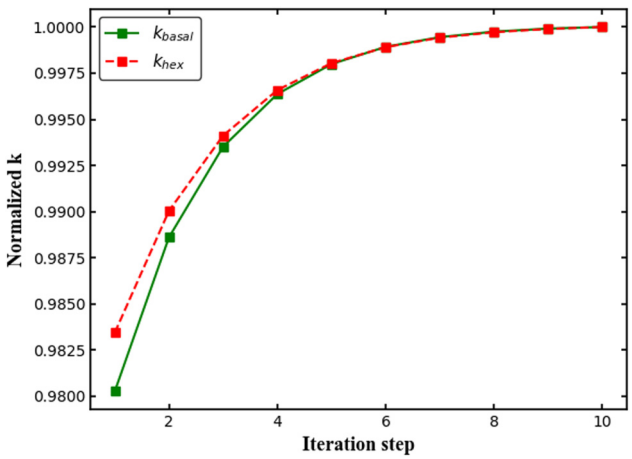

FIG. 3. The convergence of thermal conductivity of α-quartz as a function of iteration step at 300 K and 1 GPa, normalized to the value after 10 iterations.

III. RESULT AND DISCUSSION

A. Anisotropy of thermal conductivity

The thermal conductivities of α-quartz silica were measured at atmospheric pressure;[6,9] this can be used to validate our calculations, as shown in Fig. 4. The thermal conductivity tensor of the

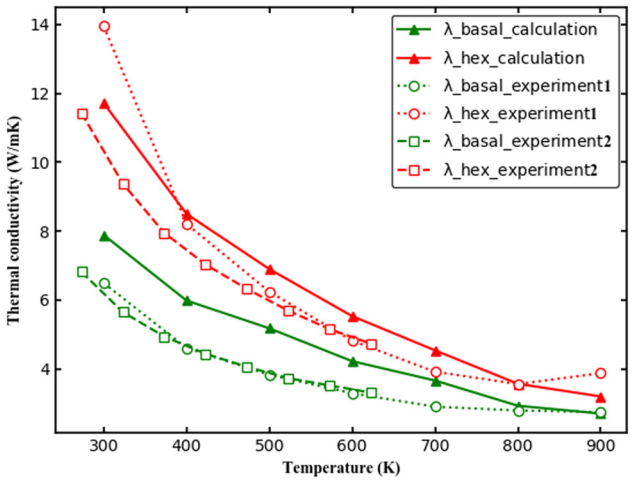

FIG. 4. Comparison of the calculated (solid triangles) and experimentally measured thermal conductivity (Ref. 9, hollow circles; Ref. 6, hollow squares) as a function of temperature. The results of basal and hexagonal directions are given in green and red, respectively.

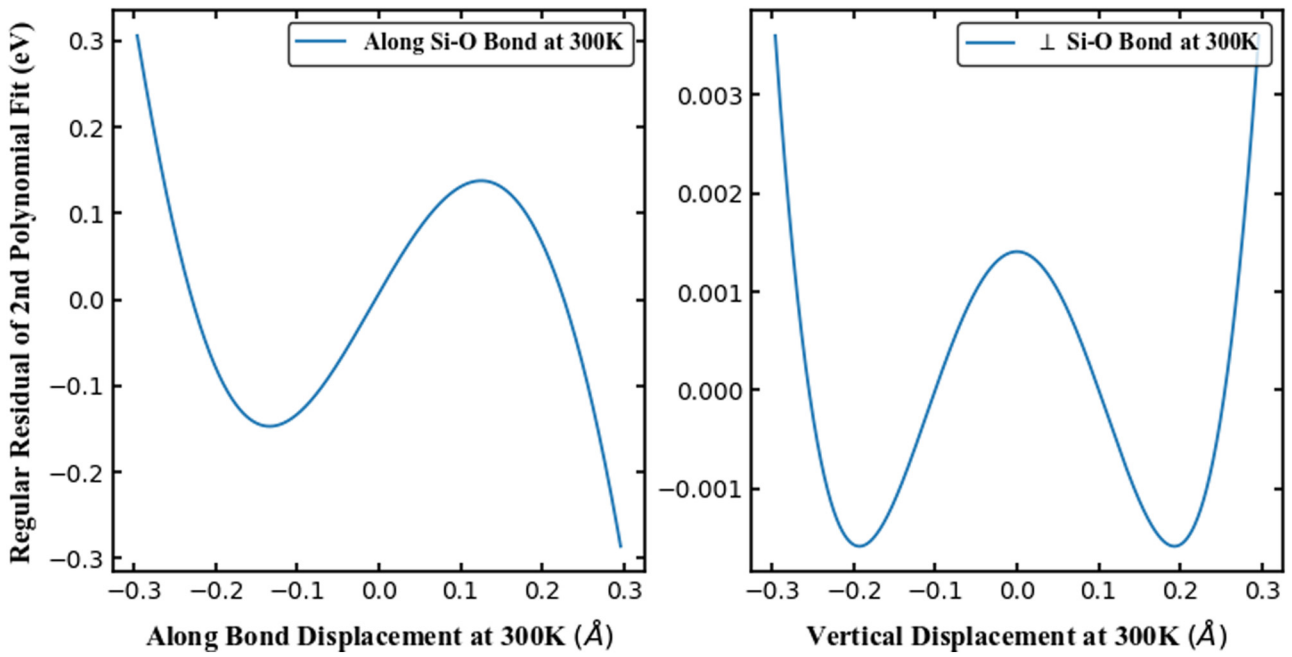

FIG. 5. Regular residuals of the second polynomial fitting to the potential energy vs the atomic displacement perturbation (a) along and (b) perpendicular to the Si–O bonds at a temperature of 300 K and a pressure of 0 GPa.

orthorhombic structure is diagonal; thus, it is convenient to speak of the thermal conductivity along the direction, for which it is implied that the thermal gradient lies in the same direction as the thermal current. There are significant differences between the two experimental determinations of the thermal conductivity along the hexagonal direction (open red symbols), particularly at low temperatures. For thermal conductivity in the basal plane, the two sets of experiments (open green symbols) agree better. The computed values of the thermal conductivities (for a pressure of 0 GPa and over the temperature range of 300–900 K) are in reasonable agreement with the experimental results, both in the numerical values and their trend with respect to temperature. In general, the computed values are larger than the experimental results. One of the reasons might be that the calculation model is a perfect crystal without impurities, which decreases the thermal conductivity of the experimental samples.[28,29] Moreover, radiative heat transfer may be important at high temperature.[9] Its non-negligible contribution to the thermal conductivity might be the reason for the increase of experimental thermal conductivity at temperature above 800 K.

Another possible origin of the difference between the experimental and computed values is the limitation of the computational approach to three-phonon processes. To assess the contribution of four- and more-phonon processes, which would further reduce the thermal conductivity, the fourth-order phonon anharmonicity was analyzed by calculating the residual. The residual is defined as the difference between the potential energy and the second-order polynomial fit to the potential as a function of the atomic displacement perturbation.[30] The residual of perturbations along the Si–O bond at 300 K and 0 GPa is shown in Fig. 5(a). The antisymmetric shape of this means that the fourth-order potential energy is negligible compared to the third-order term along the Si–O bond. In contrast, the residual shape perpendicular to the Si–O bond is W-like in Fig. 5(b), indicating that there is a fourth-order contribution. However, the magnitude of the deviations is very small, indicating that these four-phonon processes are small. The factor of ~100 between the size of the deviations in Figs. 5(a) and 5(b) may seem surprising. However, in Ref. 25, it was found that the magnitude of the residual along the Ge–Ge bond is around 20 times larger than that perpendicular to the Ge–Ge bond. Our difference for Si–O is larger, because the bond length of Si–O (1.63 Å) is shorter than that of Ge–Ge (2.41 Å), while the displacement of atoms is very similar (maximum 0.3 Å).

The thermal conductivities along the hexagonal axis ([0001]) of α-quartz are larger than along the basal directions ([1000], [0100]), which is consistent with the characteristics of a positive uniaxial crystal. From the spectral thermal conductivity of α-quartz at 300 K and 0 GPa as shown in Fig. 6, we can see that larger conductivity along the hexagonal direction comes largely from the phonons with frequencies between 2 THz and 7 THz.

B. The effect of temperature on thermal conductivity

In Figs. 7(a) and 7(b), we show the temperature dependence of the thermal conductivity for three different pressures. For all pressures, the thermal conductivity decreases with increasing

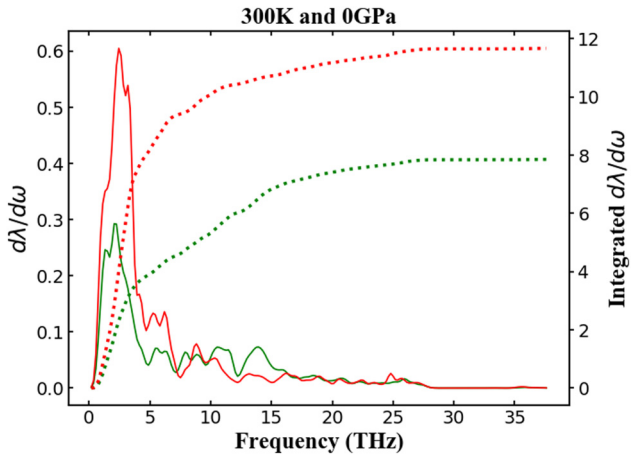

FIG. 6. Spectral thermal conductivity (solid line) along the hexagonal axis (red) and in the basal direction (green) and frequency integrated values (dashed lines) of α-quartz at 300 K and 0 GPa.

temperature along both the hexagonal and the basal directions, with the decrease in the hexagonal direction being larger. As a result, the ratio of the hexagonal to basal thermal conductivity, i.e., the anisotropy, decreases with increasing temperatures as shown in Fig. 7(c).

C. The effect of pressure on thermal conductivity

In Figs. 8(a) and 8(b), the thermal conductivity is plotted as a function of pressure at four different temperatures. The effect of pressure on the thermal conductivity is positive and linear both along the hexagonal and basal directions, while the effect of temperature is negative and nonlinear as shown in Figs. 7(a) and 7(b). The pressure also enhances the anisotropy of the thermal conductivity, as the ratio between the values along two directions increases in Fig. 8(c). The effect of pressure on anisotropy can be explained by Young's modulus, which was calculated using the BKS potential at 0 K. Young's modulus in the basal direction is 80.4 GPa and in the hexagonal direction is 102.4 GPa, both of which are very close to the experiment values of 79.4 GPa and 102.8 GPa.[31] The stiffer direction was influenced more by pressure.

In Figs. 7(a) and 7(b), the thermal conductivity shows a power-law dependence on temperature and a linear dependence on pressure in Figs. 8(a) and 8(b). Therefore, a function of type $\lambda = C(P)T^{\alpha}$ $l = C(P)T^{a}$ is fitted using the nonlinear least squares method. The exponent of temperature for the hexagonal direction is close to -1 for both systems. The function $C(P)$ is approximately linear in pressure. The detailed parameters are shown in Table I.

Another prevalent way to present the temperature and pressure dependence of the thermal conductivity is as $\lambda = \lambda_0(1 + BP)/(1 + AT)$. For the basal direction, this formula yields the reasonable fit of $\lambda_0 = 55.43$ W/m K, A = 0.02 K^{-1}, and B = 0.07 $(GPa)^{-1}$. When we performed the same fit for the hexagonal direction, physically unreasonable values of the parameters were obtained. We ascribed this to the extreme sensitivity of the fit to slight variations in the data.

D. Analysis

Figure 9 shows the calculated dispersion relationship and phonon density of states (DOS) at 0 K and 0 GPa, using the BKS

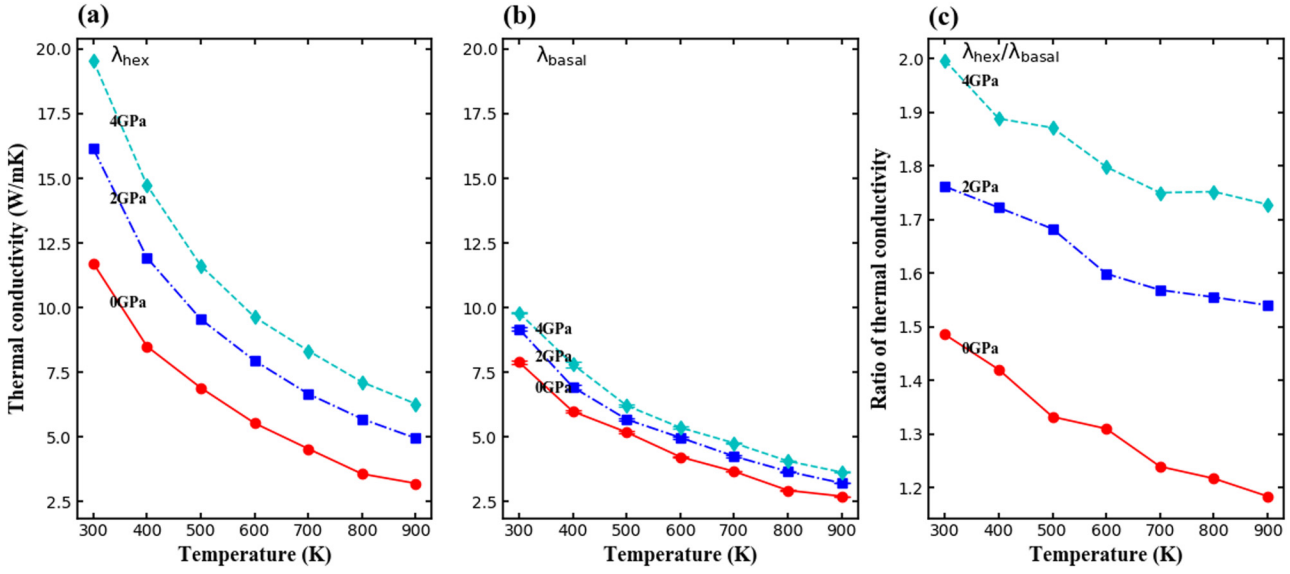

FIG. 7. The thermal conductivities of α-quartz silica as a function of temperature at 0 GPa, 2 GPa, and 4 GPa and the ratio of hexagonal to basal direction.

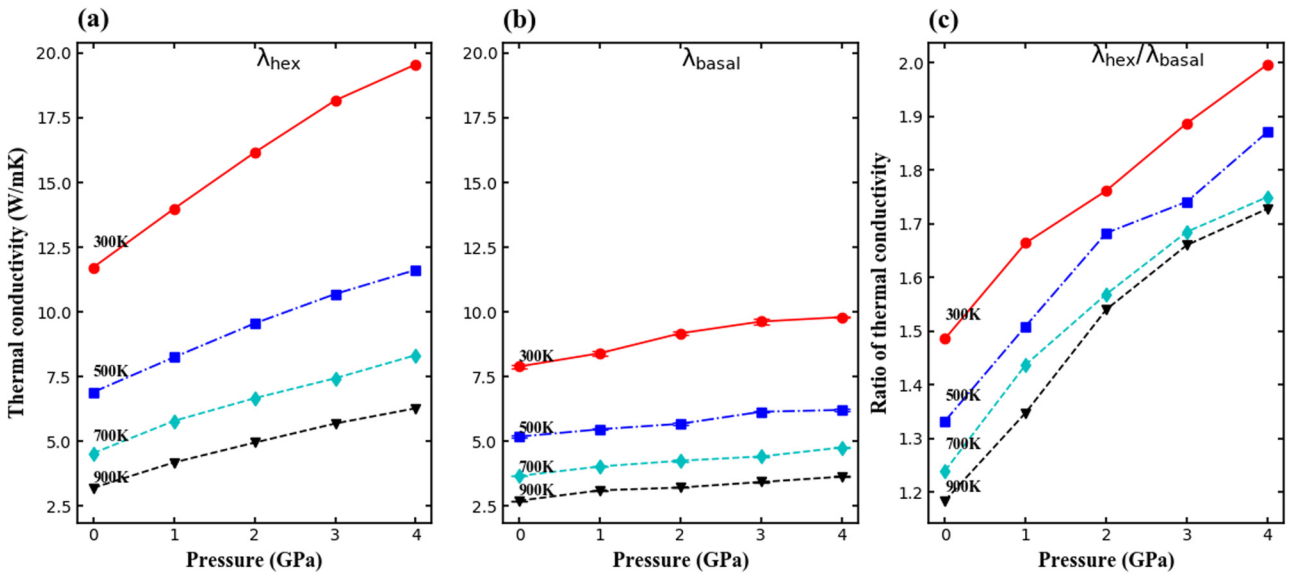

FIG. 8. The thermal conductivities of α-quartz silica as a function of pressure at 300 K, 500 K, 700 K, and 900 K and the ratio of hexagonal to basal direction.

potential. For frequencies between ~3 THz and 29 THz, the density of states is relatively flat, consistent with the rather dense and uniform phonon dispersion curves. The maximum value of DOS at 33.2 THz is associated with the very flat, high energy bands in the phonon dispersion curve.

As an evaluation of the quality of the BKS potential, a comparison of calculated and experimental dispersion curves[32] for the Γ-K direction is shown in Fig. 9. In our results, the low-frequency and high-frequency portions of the dispersion curves are close to the experimental results. The discrepancy of the middle-frequency range indicates the limitations of the BKS potential.

Generally, the effect of temperature and pressure on DOS is a shift with respect to frequency, presented as peaks and valleys alternatively appear in the DOS difference in Fig. 10. Figure 10(a) shows the DOS from Fig. 9 and defines the baseline against which to compare the effects of temperature and pressure. Figure 10(b) shows the change in the DOS as the temperature increases from 300 K to 900 K. The expansion of the lattice associated with increasing temperature has the general effect of softening the phonon modes. Thus, the first peak of DOS difference in Fig. 10(b) is upward, indicating added DOS at a frequency, which is lower than that of the first peak of DOS at 300 K in Fig. 10(a); contrariwise, the effect of pressure is to decrease the lattice parameter and increase the phonon frequencies; thus, the first peak in Fig. 10(c) is downward. With higher temperature of 900 K and pressure of 4 GPa, the volume of the unit cell is still compressed compared with a temperature of 300 K and a pressure of 0 GPa. Thus, again the first peak is downward. The strong upward and downward peaks at ~33 THz correspond to small changes in the frequency of the flat high-frequency band. The overall effect of both temperature and pressure is thus rather small. That is, we cannot expect these changes to the harmonic behavior of the phonons to explain the significant temperature and pressure dependence of the thermal conductivity.

TABLE I. The fitting parameters of thermal conductivity as a function of temperature and pressure of type $\lambda = C(P)T^a$.

Direction	$C(P)$	a
Hexagonal direction	$(5295.4 \pm 109.4) + (938.5 \pm 44.7)P$	−1.07
Basal direction	$(1430.8 \pm 17.8) + (95.0 \pm 7.26)P$	−0.91

The phonon lifetimes and the averaged values as a function of frequency are shown in Fig. 11 for temperatures of 300 K and 900 K and pressures of 0 GPa and 4 GPa. There is a dramatic initial decrease of the phonon lifetime with frequency, followed by a fluctuation within a narrow range, and then a small increase after 20 THz. As we would expect, the effect of temperature and pressure on phonon lifetime is similar to the effect on the thermal conductivity itself. Specifically, the phonon lifetimes decrease with increasing temperature [Fig. 11(b)] and increase with increasing pressure [Fig. 11(c)]. Comparing Fig. 11(a) with Fig. 6, the lifetime of the high flatband is in the same range with that of frequency from 5 THz to 10 THz. However, the contribution to the thermal conductivity is smaller because of the much lower phonon velocity. The phonon lifetime is longest when the thermal conductivity is the highest at 300 K and 4 GPa, especially in the frequency range from 0 THz to 10 THz. Under the condition of Fig. 11(d), the volume is compressed, compared to under the condition of Fig. 11(a); however, the phonon lifetime is lower. This arises from the combined effect of temperature and pressure, which changes

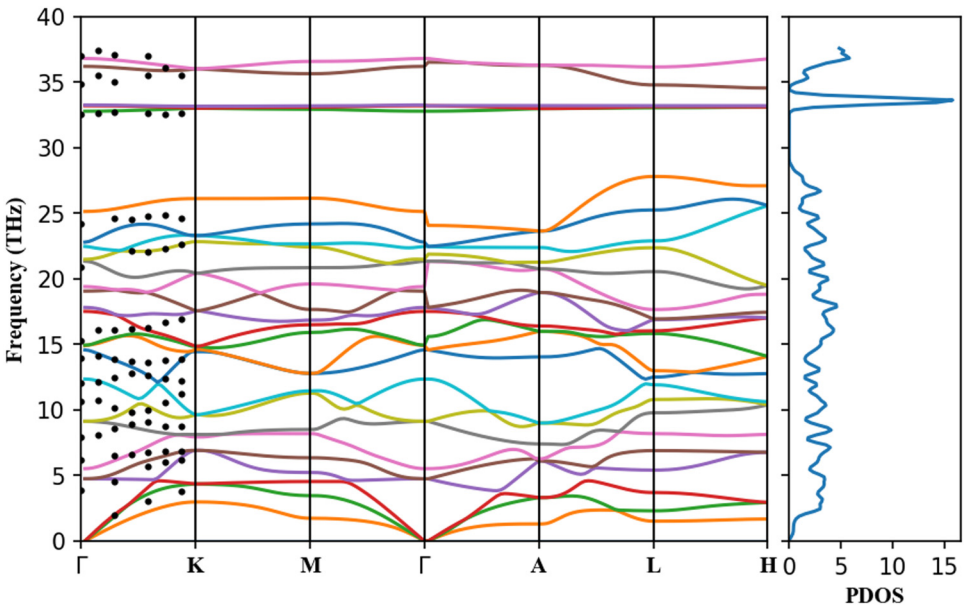

FIG. 9. The calculated dispersion relationship and phonon density of states of α-quartz. The closed circles indicate the experimental frequencies α-quartz at 0 K for the Γ-K direction.[32]

not only the average density but also the amplitude of thermal vibrations.

The normalized spectral thermal conductivity is shown in Fig. 12. Comparing Fig. 12(b) with Fig. 12(a), we can see that the phonons in 2–7 THz range frequency are the dominant contributors to the thermal conductivity. Moreover, the contribution from phonon with larger frequencies (between 18 THz and 26 THz) increases as the temperature increases. The same conclusion can be

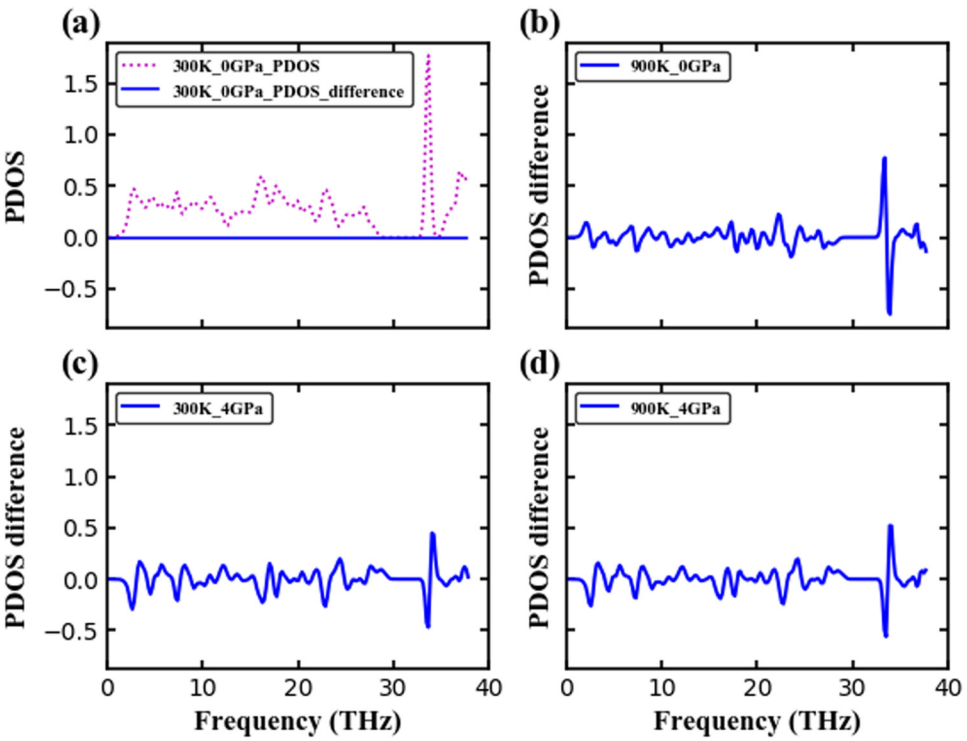

FIG. 10. (a) Phonon density of states for a temperature of 300 K and a pressure of 0 GPa. (b) Difference in DOS for a temperature of 900 K and a pressure of 0 GPa. (c) Difference in DOS for a temperature of 300 K and a pressure of 4 GPa. (d) Difference in DOS for a temperature of 900 K and a pressure of 4 GPa.

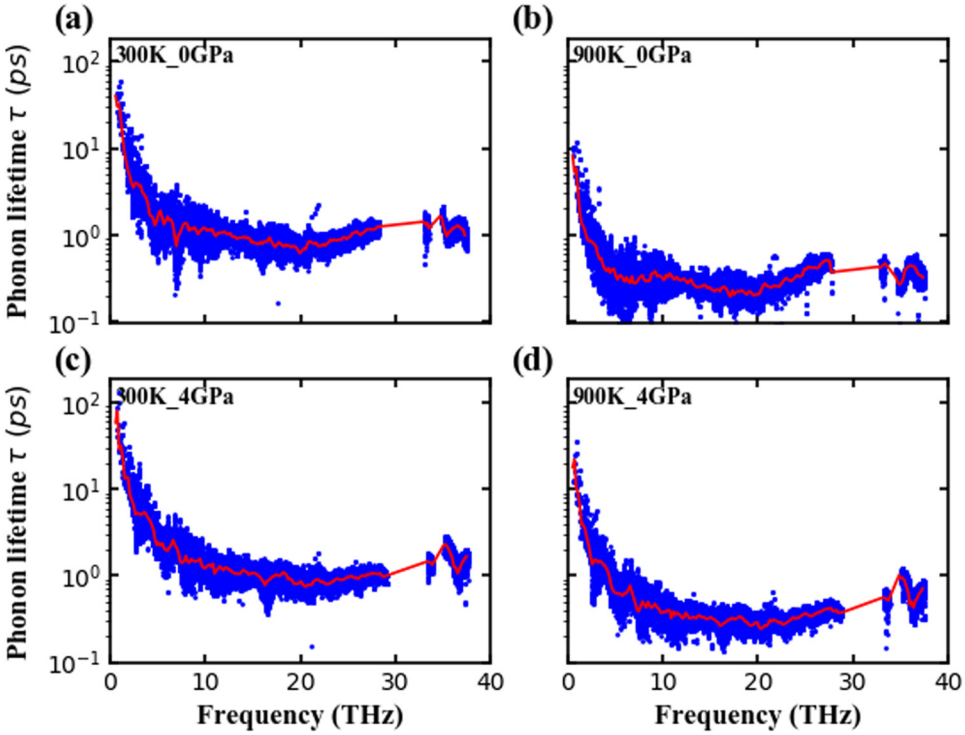

FIG. 11. Phonon lifetimes (blue dots) and the averaged values (red line) as a function of frequency for different temperatures and pressures.

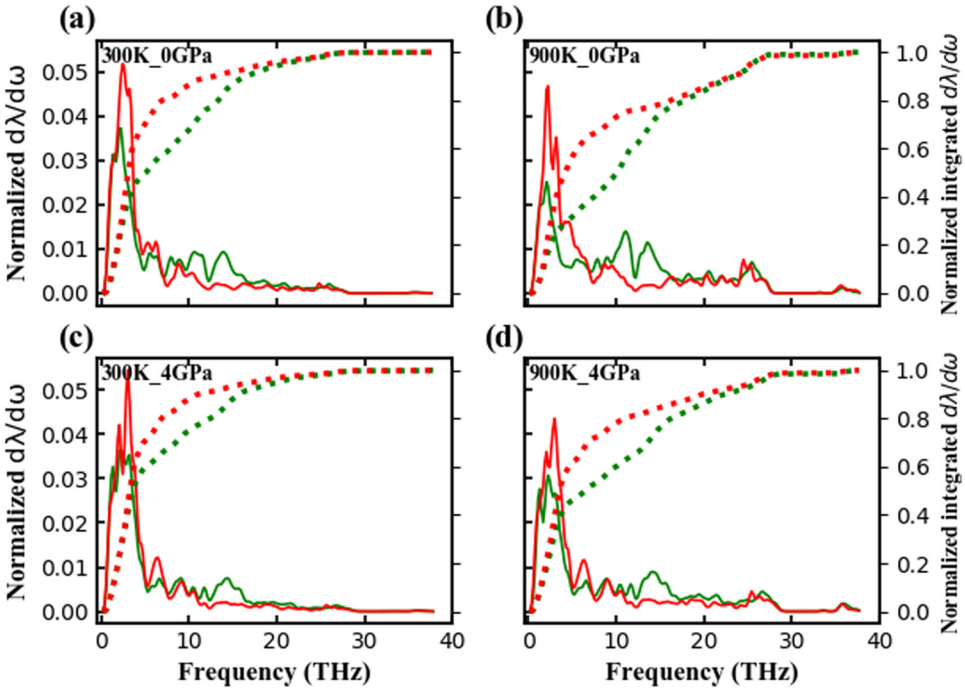

FIG. 12. The normalized spectral thermal conductivity (solid) and integrated values (dotted) of the basal (green) and hexagonal (red) directions.

TABLE II. The contribution to the basal thermal conductivity from different phonon branches.

Condition	Phonon branch		
	Acoustic branches (%)	Middle-frequency branches (%)	High-frequency branches (%)
300 K 0 GPa	48.9	50.9	0.2
300 K 4 GPa	60.2	39.6	0.2
900 K 0 GPa	30.1	68.9	1.0
900 K 4 GPa	46.1	52.4	1.5

drawn when comparing Fig. 12(d) with Fig. 12(c). For the effect of pressure on the basal thermal conductivity, the contribution from phonons with frequency between 10 THz and 16 THz decreases with increasing pressure. The effect of pressure on the thermal conductivity normal to the basal direction is not so clear but is consistent with the effect of pressure being weaker.

This analysis also allows the contribution of the various branches of the phonon dispersion curves to the thermal conductivity to be determined. These are shown in Tables II and III. The dispersion curves are divided into three groups: acoustic branches, middle-frequency branches (between acoustic branches and 30 THz), and high-frequency branches (flatbands above 30 THz). The contribution of the acoustic branches to the thermal conductivity increases with higher pressure or lower temperature. The trend of contribution of middle-frequency branches is opposite. The flat high-frequency branches contribute little to the thermal conductivity because their velocity is very low. The acoustic branches contribute a higher percentage to the thermal conductivity in the hexagonal direction than in the basal direction.

TABLE III. The contribution to the hexagonal thermal conductivity from different phonon branches.

Condition	Phonon branch		
	Acoustic branches (%)	Middle-frequency branches (%)	High-frequency branches (%)
300 K 0 GPa	68.5	31.3	0.2
300 K 4 GPa	71.2	28.7	0.1
900 K 0 GPa	52.3	46.2	1.5
900 K 4 GPa	61.7	37.2	1.1

IV. CONCLUSIONS

By solving the Boltzmann transport equation with interatomic interactions described by the BKS potential, we have elucidated the effects of temperature and pressure on the thermal conductivity of α-quartz. The results of the thermal conductivities at atmospheric pressure are in reasonable agreement with the experimental results, both for the anisotropy of basal and hexagonal directions, and their trends with respect to temperature. Temperature has a negative effect on thermal conductivity and reduces the difference between the basal and hexagonal directions, whereas pressure has a positive effect and enhances the anisotropy. The changes in the harmonic lattice dynamics due to the variation of temperature and pressure, such as phonon density of states, have little effect. Rather, the anharmonic lattice effects, such as the perturbation of the phonon distribution function, determine the heat conduction along both the basal and hexagonal directions. The contribution of the acoustic branches to the thermal conductivity increases in both directions, as temperature decreases or pressure increases. The contribution of phonon branches in midrange frequencies is nearly unchanged in the hexagonal direction and increases with increasing temperature and decreasing pressure in the basal direction.

ACKNOWLEDGMENTS

The support from the National Natural Science Foundation of China (NNSFC) (Grant No. 51720105007) is greatly acknowledged.

REFERENCES

[1]D. S. Chapman, "Thermal gradients in the continental crust," Geol. Soc. London Spec. Publ. **24**(1), 63–70 (1986).
[2]S. Fuchs, H.-J. Förster, K. Braune, and A. Förster, "Calculation of thermal conductivity of low-porous, isotropic plutonic rocks of the crust at ambient conditions from modal mineralogy and porosity: A viable alternative for direct measurement?," J. Geophys. Res. Solid Earth **123**(10), 8602–8614 (2018).
[3]R. K. Workman and S. R. Hart, "Major and trace element composition of the depleted MORB mantle (DMM)," Earth Planet. Sci. Lett. **231**(1), 53–72 (2005).
[4]D. L. Anderson, *New Theory of the Earth* (Cambridge University Press, Cambridge, 2007).
[5]R. S. Anderson and S. P. Anderson, *Geomorphology: The Mechanics and Chemistry of Landscapes* (Cambridge University Press, Cambridge, 2010).
[6]C. Clauser and E. Huenges, *Thermal Conductivity of Rocks and Minerals* (American Geophysical Union, Washington DC, 1995), Vol. 3.
[7]Y.-G. Yoon, R. Car, D. J. Srolovitz, and S. Scandolo, "Thermal conductivity of crystalline quartz from classical simulations," Phys. Rev. B **70**(1), 12302 (2004).
[8]A. J. H. McGaughey and M. Kaviany, "Thermal conductivity decomposition and analysis using molecular dynamics simulations: Part II. Complex silica structures," Int. J. Heat Mass Transf. **47**(8), 1799–1816 (2004).
[9]H. Kanamori, N. Fujii, and H. Mizutani, "Thermal diffusivity measurement of rock-forming minerals from 300° to 1100°K," J. Geophys. Res. **73**(2), 595–605 (1968).
[10]A. France-Lanord, P. Soukiassian, C. Glattli, and E. Wimmer, "Ab initio parameterization of a charge optimized many-body forcefield for Si–SiO_2: Validation and thermal transport in nanostructures," J. Chem. Phys. **144**(10), 104705 (2016).
[11]E. H. Ratcliffe, "Thermal conductivities of fused and crystalline quartz," Br. J. Appl. Phys. **10**(1), 22–25 (1959).
[12]H. Birch and H. Clark, "The thermal conductivity of rocks and its dependence upon temperature and composition; part II," Am. J. Sci. **238**(9), 613–635 (1940).

[13]H. Birch and H. Clark, "The thermal conductivity of rocks and its dependence upon temperature and composition," Am. J. Sci. **238**(8), 529–558 (1940).
[14]I. M. Abdulagatov, S. N. Emirov, T. A. Tsomaeva, K. Gairbekov, S. Y. Askerov, and N. A. Magomedova, "Thermal conductivity of fused quartz and quartz ceramic at high temperatures and high pressures," J. Phys. Chem. Solids **61**(5), 779–787 (2000).
[15]R. E. Cohen, "Thermal conductivity of MgO at high pressures," Rev. High Press. Sci. Technol. **7**, 160–162 (1998).
[16]N. de Koker, "Thermal conductivity of MgO periclase from equilibrium first principles molecular dynamics," Phys. Rev. Lett. **103**(12), 125902 (2009).
[17]S. Stackhouse, L. Stixrude, and B. B. Karki, "Thermal conductivity of periclase (MgO) from first principles," Phys. Rev. Lett. **104**(20), 208501 (2010).
[18]E. G. Jones and C. H. Lineweaver, "To what extent does terrestrial life 'follow the water'?," Astrobiology **10**(3), 349–361 (2010).
[19]A. F. Wright and M. S. Lehmann, "The structure diffraction of quartz at 25 and 590°C determined by neutron diffraction," J. Solid State Chem. **36**, 371–380 (1981).
[20]B. W. H. van Beest, G. J. Kramer, and R. A. van Santen, "Force fields for silicas and aluminophosphates based on ab initio calculations," Phys. Rev. Lett. **64**(16), 1955–1958 (1990).
[21]K. Kihara, "A X-ray study of the temperature dependence of the quartz structure," Eur. J. Miner. **2**, 63–77 (1990).
[22]H. Kimizuka, H. Kaburaki, and Y. Kogure, "Molecular-dynamics study of the high-temperature elasticity of quartz above the α-β phase transition," Phys. Rev. B Condens. Matter Mater. Phys. **67**(2), 1–7 (2003).
[23]M. H. Muser and K. Binder, "Molecular dynamics study of the alpha-beta transition in quartz: Elastic properties, finite size effects, and hysteresis in the local structure," Phys. Chem. Miner. **28**(10), 746–755 (2001).
[24]J. R. Smyth and C. J. Hatton, "A coesite-sanidine grospydite from the Roberts Victor kimberlite," Earth Planet. Sci. Lett. **34**(2), 284–290 (1977).
[25]B. Kunal and G. Jibamitra, "Quartz-coesite transition revisited: Reversed experimental determination at 500–1200°C and retrieved thermochemical properties," Am. Mineral. **80**, 231 (1995).
[26]A. Chernatynskiy and S. R. Phillpot, "Phonon transport simulator (PhonTS)," Comput. Phys. Commun. **192**, 196–204 (2015).
[27]A. Chernatynskiy and S. R. Phillpot, "Evaluation of computational techniques for solving the Boltzmann transport equation for lattice thermal conductivity calculations," Phys. Rev. B Condens. Matter Mater. Phys. **82**(13), 1–17 (2010).
[28]M. Yao, T. Watanabe, P. Schelling, P. Keblinski, D. Cahill, and S. Phillpot, "Phonon-defect scattering in doped silicon by molecular dynamics simulation," J. Appl. Phys. **104**, 24905 (2008).
[29]R. E. Jones and D. K. Ward, "Influence of defects on the thermal conductivity of compressed LiF," Phys. Rev. B **97**(5), 54103 (2018).
[30]S. Y. Yue, X. Zhang, G. Qin, S. R. Phillpot, and M. Hu, "Metric for strong intrinsic fourth-order phonon anharmonicity," Phys. Rev. B **95**(19), 195203 (2017).
[31]P. Heyliger, H. Ledbetter, and S. Kim, "Elastic constants of natural quartz," J. Acoust. Soc. Am. **114**(2), 644–650 (2003).
[32]D. Strauch and B. Dorner, "Lattice dynamics of alpha -quartz. I. Experiment," J. Phys. Condens. Matter **5**(34), 6149–6154 (1993).